Textile & Leather Review

ISSN 2623-6281 | www.tlr-journal.com | 10.31881/TLR

Spatiotemporal Convolutional Network-Based Distributed Secondary Cooperative Restoration Control of Frequency and Voltage in Microgrids

Ziyue Zhou

How to cite: Zhou Z. Spatiotemporal Convolutional Network-Based Distributed Secondary Cooperative Restoration Control of Frequency and Voltage in Microgrids. Textile & Leather Review. 2026; 9:3899-3929. https://doi.org/10.31881/TLR.2026.3899

How to link: https://doi.org/10.31881/TLR.2026.3899

Published: 25 April 2026

Spatiotemporal Convolutional Network-Based Distributed Secondary Cooperative Restoration Control of Frequency and Voltage in Microgrids

Ziyue Zhou

Changkong College, Nanjing University of Aeronautics and Astronautics, Nanjing, 211106, China.
zhouzy@nuaa.edu.cn

Article
https://doi.org/10.31881/TLR.2026.3899
Published 25 April 2026

ABSTRACT

To address the limited capability of conventional distributed secondary control methods in exploiting multi-node coupling and dynamic information during frequency and voltage restoration in islanded microgrids, this paper proposes a spatiotemporal convolutional network-based distributed secondary restoration control method. First, a microgrid model incorporating droop control, communication topology, and restoration objectives is established, and the restoration problem is formulated as a distributed control task based on local measurements and neighborhood information. Then, spatiotemporal input features integrating frequency and voltage deviations and power information are constructed. A spatiotemporal convolutional network is employed to extract spatial correlation among distributed generators and temporal characteristics during disturbances, thereby generating secondary compensation signals. Furthermore, a hybrid control framework combining a distributed secondary controller with a spatiotemporal compensator is developed to enhance regulation capability while preserving the control structure. Simulation results show that the proposed approach achieves smaller deviations, shorter recovery times, and stronger disturbance rejection under load variations, parameter perturbations, and communication delays. The results indicate that introducing spatiotemporal feature modeling into distributed secondary control reduces transient deviations, shortens recovery time, and improves disturbance rejection capability in the tested microgrid scenarios.

KEYWORDS

microgrid, distributed secondary control, spatiotemporal convolutional network, cooperative frequency and voltage restoration

INTRODUCTION

With the rapid development of distributed energy resources, energy storage systems, and power electronic interfacing technologies, microgrids have emerged as an important solution for enhancing renewable energy

integration, improving distribution system flexibility, and ensuring reliable power supply [1, 2]. In particular, under islanded operating conditions, microgrids are capable of autonomous power supply and local energy management, which makes them highly promising for remote-area electrification, critical load support, and the development of future power systems [3, 4]. In general, inverter-based distributed generators are operated under a hierarchical control architecture to achieve stable operation and proper power regulation [5]. Among these control layers, primary droop control has been widely adopted due to its simple implementation and low communication requirements [6, 7]. However, while droop control enables active and reactive power sharing, it inevitably leads to deviations in system frequency and voltage magnitude from their nominal values. Therefore, high-performance secondary control strategies are essential to restore frequency and voltage rapidly and accurately, thereby guaranteeing power quality and operational stability in islanded microgrids.

In recent years, extensive research efforts have been devoted to secondary control of microgrids. Centralized secondary control can achieve high control accuracy by utilizing global information, but it strongly depends on a central controller and communication infrastructure, which makes it vulnerable to single-point failures and limits its scalability [8]. By contrast, distributed secondary control has attracted increasing attention because of its superior flexibility, robustness, and scalability [9]. Existing distributed approaches are mainly developed based on consensus algorithms, proportional-integral regulation, state-feedback strategies, and event-triggered mechanisms, which can restore frequency and voltage to a certain extent while maintaining power-sharing performance. Nevertheless, as microgrid structures become increasingly complex and the coupling among distributed generators becomes stronger, conventional control schemes still show limited capability in exploiting the spatial correlations among multiple nodes and the temporal dynamic characteristics during disturbance transients. In addition, frequency restoration and voltage restoration are often treated in a relatively decoupled manner, and their intrinsic coordination mechanisms have not been fully utilized. This limitation may further restrict the improvement of dynamic performance and overall control effectiveness [10, 11].

To address the above issues, this paper proposes a spatiotemporal convolutional network-based distributed secondary cooperative restoration control method for frequency and voltage in microgrids. The proposed method is developed for the coordinated control of multiple distributed generators in islanded microgrids, where a feature representation model is constructed to jointly capture spatial correlations among DG nodes and temporal dependencies over a finite historical window. In this paper, “spatiotemporal” specifically refers

to the combination of node-to-node coupling described by the communication/electrical neighborhood and the time-sequential variations of frequency, voltage, and power variables within the sliding window. Based on this representation, a distributed secondary control framework is designed to generate cooperative compensation signals for frequency and voltage restoration. Compared with conventional approaches that rely mainly on instantaneous errors or fixed control laws, the proposed method can extract spatiotemporal response features from the operating scenarios covered by the training dataset, thereby reducing transient deviations, shortening recovery time, and improving disturbance rejection capability within the considered operating range. Furthermore, the effectiveness of the proposed approach will be systematically investigated through system modeling, controller design, stability analysis, and comprehensive case studies under multiple operating conditions.

SYSTEM MODELING AND PROBLEM FORMULATION

Microgrid Structure and Primary Control

Consider an islanded AC microgrid composed of N inverter-based distributed generators (DGs), local loads, and distribution lines [12, 13]. The DG units are coupled through the electrical network for power exchange and interact through a communication network to support the implementation of distributed secondary control. To ensure stable operation, a hierarchical control architecture is adopted, where the primary control layer is responsible for active and reactive power regulation as well as preliminary power sharing, while the secondary control layer is employed to restore system frequency and voltage to their nominal values.

For the i -th DG, the primary droop control law can be described as:

$$\omega_i = \omega^* - m_{p_i}(P_i - P_i^*) \tag{1}$$

$$V_i = V^* - n_{q_i}(Q_i - Q_i^*) \tag{2}$$

where ω_i and V_i denote the output frequency and voltage magnitude of the i -th DG, respectively, ω^* and V^* are the nominal system frequency and voltage, P_i and Q_i represent the active and reactive power outputs, P_i^* and Q_i^* are the corresponding reference values, and m_{p_i} and n_{q_i} are the active-power/frequency and reactive-power/voltage droop coefficients, respectively.

It can be seen from the above equations that primary droop control enables power regulation and sharing without requiring high-speed communication [14]. However, this benefit comes at the cost of steady-state deviations in frequency and voltage when load conditions change. Therefore, primary control alone is insufficient to meet the requirements of high-quality power supply and accurate system regulation, and an additional secondary control mechanism is required to provide compensation for frequency and voltage restoration.

For consistency, u_i^{ω} and u_i^{V} are used throughout this paper to denote the frequency and voltage secondary compensation signals, respectively. Then, the control laws augmented by secondary control can be written as:

$$\omega_i = \omega^* - m_{p_i}(P_i - P_i^*) + u_i^{\omega} \tag{3}$$

$$V_i = V^* - n_{q_i}(Q_i - Q_i^*) + u_i^{V} \tag{4}$$

where u_i^{ω} and u_i^{V} are generated by the designed distributed secondary controller to achieve cooperative restoration of frequency and voltage.

Communication Topology and Distributed Information Exchange

To coordinate information exchange among multiple DG units, an undirected communication graph $\mathcal{G} = (\mathcal{V}, \mathcal{E})$ is introduced to describe the distributed communication network, where the node set $\mathcal{V} = \{1, 2, ..., N\}$ represents all DG units and the edge set $\mathcal{E} \subseteq \mathcal{V} \times \mathcal{V}$ denotes the communication links among them. If there exists a communication link between node i and node j , then $(i, j) \in E$.

Let $A = [a_{ij}] \in \mathbb{R}^{N \times N}$ denote the adjacency matrix, where $a_{ij} = 1$ if node j can transmit information to node i , and $a_{ij} = 0$ otherwise. The degree matrix is defined as $D = diag(d_1, d_2, ..., d_N)$, where $d_i = \sum_{j=1}^{N} a_{ij}$. Accordingly, the Laplacian matrix is given by:

$$L = D - A \tag{5}$$

For the i -th DG, the set of its neighboring nodes is defined as

$$\mathcal{N}_i = \{ j \in \mathcal{V} \mid a_{ij} = 1 \} \tag{6}$$

Under the distributed control framework, each DG makes its control decision using only local measurements and limited information received from its neighboring nodes, without relying on any centralized global information. Specifically, the i -th DG can access its local frequency deviation $\Delta\omega_i = \omega_i - \omega^*$, voltage deviation $\Delta V_i = V_i - V^*$, active/reactive power outputs P_i and Q_i , as well as the corresponding local states of its neighbors. This information exchange pattern provides the control architecture with good scalability and resilience against single-point failures, while also laying the foundation for subsequent control design based on spatiotemporal feature extraction.

Secondary Control Objectives

The objective of this study is to develop a distributed secondary control strategy for islanded microgrids such that each DG can achieve cooperative restoration of frequency and voltage using only local measurements and neighborhood communication, while maintaining satisfactory dynamic performance. Specifically, the secondary control objectives can be summarized as follows.

First, the system frequency should be restored to its nominal value, i.e., for all DG units,

$$\lim_{t\to\infty} \omega_i(t) = \omega^*, i = 1, 2, ..., N \tag{7}$$

Second, the output voltage of each DG should be restored to its nominal value, namely,

$$\lim_{t\to\infty} V_i(t) = V^*, i = 1, 2, ..., N \tag{8}$$

Third, while restoring frequency and voltage, the controller should preserve the desirable power-sharing characteristics established by the primary control layer as much as possible, so as to avoid introducing significant active/reactive power-sharing errors through the secondary compensation process. In addition, the designed controller is expected to exhibit fast dynamic response, low overshoot, and strong disturbance rejection capability, so as to meet the control requirements under load fluctuations, parameter perturbations, and other complex operating conditions.

It should be noted that although frequency restoration and voltage restoration can be defined as separate control objectives, they are not completely independent in practical microgrid operation [15]. On the one hand, active and reactive power regulation jointly affect the system dynamics through network coupling. On the other hand, the DG units are interconnected through both electrical and communication networks,

which gives rise to multi-node coupling effects. Therefore, if both the spatial correlation among nodes and the temporal evolution of system responses can be exploited simultaneously in the secondary control design, the coordinated restoration performance of frequency and voltage is expected to be further improved.

Problem Formulation

Based on the above system model and control objectives, this paper addresses the following problem: for an islanded AC microgrid consisting of multiple inverter-based DGs, and under a given communication topology satisfying basic connectivity requirements, how can a spatiotemporal convolutional network-based distributed secondary controller be designed such that each DG generates the frequency compensation signal u_i^{ω} and the voltage compensation signal u_i^{V} online using only local measurements and neighboring information, thereby achieving fast and coordinated restoration of system frequency and voltage?

Furthermore, considering that microgrid dynamics under disturbances exhibit both strong inter-node coupling and significant temporal evolution characteristics, the local operating states of all DGs over a continuous time window are organized as spatiotemporal input features. For the i -th DG, the input at time t can be expressed as:

$$\mathbf{X}_i(t) = [\mathbf{x}_i(t-T+1), \mathbf{x}_i(t-T+2), ..., \mathbf{x}_i(t)] \tag{9}$$

where T denotes the time-window length, and $x_i(t)$ is the feature vector composed of local states and neighborhood information. For example, it can be defined as:

$$\mathbf{x}_i(t) = [\Delta\omega_i(t), \Delta V_i(t), P_i(t), Q_i(t), \{\Delta\omega_j(t), \Delta V_j(t)\}_{j\in\mathcal{N}_i}] \tag{10}$$

Accordingly, the objective of this paper can be further formulated as constructing a nonlinear mapping:

$$[u_i^{\omega}(t), u_i^{V}(t)] = f_{\theta}(\mathbf{X}_i(t)) \tag{11}$$

where $f_{\theta}(\cdot)$ denotes the distributed control mapping parameterized by the spatiotemporal convolutional network. Through this mapping, the controller can comprehensively exploit historical dynamic information and inter-node coupling characteristics to generate cooperative compensation signals for frequency and

voltage restoration. The subsequent sections will focus on the construction of this control mapping, closed-loop stability analysis, and control performance evaluation.

STCN-BASED DISTRIBUTED SECONDARY COOPERATIVE CONTROL DESIGN

Overall Control Framework

Based on the system model and control objectives established in Section 2, this paper develops a spatiotemporal convolutional network (STCN)-based distributed secondary cooperative restoration control framework. The proposed framework is designed for coordinated operation of multiple DG units in islanded microgrids. By simultaneously exploiting the spatial coupling among nodes and the temporal dynamic characteristics during disturbances, it generates online secondary compensation signals for frequency and voltage, thereby improving both the dynamic and steady-state performance of system restoration.

The proposed control framework mainly consists of three parts: a local measurement and neighborhood information exchange module, a spatiotemporal feature extraction module, and a distributed secondary compensation generation module. First, each DG collects its local operating information in real time, including frequency deviation, voltage deviation, active power, and reactive power, while receiving local state information from neighboring nodes through the communication network. Then, the local and neighborhood data over a continuous time window are organized into a spatiotemporal input tensor and fed into the STCN for feature extraction. Finally, the output layer of the network generates the frequency compensation signal u_i^{ω} and the voltage compensation signal u_i^{V} , which are injected into the primary droop control reference channels to realize coordinated restoration of frequency and voltage.

Unlike conventional distributed secondary control strategies, which typically construct fixed consensus terms or proportional-integral regulation terms directly from instantaneous deviations, the proposed approach explicitly models both the temporal evolution of the dynamic process and the spatial correlation among nodes. In this way, the controller can better characterize the dynamic response of the microgrid under disturbances. To avoid the potential stability risks associated with a purely data-driven controller, the STCN output is designed as a cooperative compensation term embedded into the secondary control channel, so that the proposed method preserves the basic distributed control structure while enhancing dynamic regulation capability.

Spatiotemporal Feature Construction

The effectiveness of the STCN controller critically depends on the construction of input features. Since the frequency and voltage restoration process in microgrids exhibits both strong temporal dependence and inter-node coupling, a sliding time-window mechanism is adopted to organize the operating states of DGs over multiple consecutive sampling instants into spatiotemporal input features.

For the i -th DG, the local feature vector at time t is defined as:

$$\mathbf{x}_i(t) = [\Delta\omega_i(t), \Delta V_i(t), P_i(t), Q_i(t)] \tag{12}$$

where $\Delta\omega_i(t) = \omega_i(t) - \omega^*$ and $\Delta V_i(t) = V_i(t) - V^*$. To reflect neighborhood coupling, the state information of neighboring nodes is further incorporated into the input, leading to the enhanced feature representation:

$$\tilde{\mathbf{x}}_i(t) = [\mathbf{x}_i(t), \{\mathbf{x}_j(t)\}_{j\in\mathcal{N}_i}] \tag{13}$$

Based on this representation, for a time window of length T , the sequential input matrix of the i -th DG is constructed as:

$$\mathbf{X}_i(t) = [\tilde{\mathbf{x}}_i(t-T+1), \tilde{\mathbf{x}}_i(t-T+2), ..., \tilde{\mathbf{x}}_i(t)] \tag{14}$$

To unify the multi-node input form, the states of all DGs within the same time window can be further organized into a global spatiotemporal input tensor:

$$\mathbf{X}(t) \in \mathbb{R}^{N\times F\times T} \tag{15}$$

where N denotes the number of DG nodes, F is the feature dimension of each node, and T is the time-window length. The three dimensions of this tensor correspond to the node-space dimension, the state-feature dimension, and the time dimension, respectively. Through this construction, the network is able to simultaneously learn: 1) the spatial interactions among different DG nodes; 2) the coupling among frequency, voltage, and power variables; and 3) the temporal evolution of system states after disturbances.

It should be noted that the input variables are not limited to the basic state quantities listed above. In practical implementations, other measurable variables, such as voltage phase angles, neighborhood error terms, and power-sharing deviation terms, may also be incorporated depending on the desired modeling fidelity and measurement availability. Nevertheless, for the sake of controller simplicity and engineering practicality, this paper adopts a compact core feature set consisting of frequency deviation, voltage deviation, and active/ reactive power outputs.

STCN Architecture Design

To effectively extract the spatial correlation and temporal dynamic characteristics of the multi-node microgrid system, an STCN control network is constructed with four main components: a spatial convolution module, a temporal convolution module, a feature fusion module, and an output mapping module. In order to improve reproducibility, the detailed implementation of the STCN used in this study is specified as follows. The network takes the spatiotemporal state tensor $X(t) \in \mathbb{R}^{N\times F\times T}$ as input, where $N=4$, $F=4$, and $T=12$ in the case studies. The same STCN parameters are shared by all DG units, and the distributed implementation is realized by masking the spatial aggregation according to the communication adjacency matrix. The output dimension of the network is $2N$, corresponding to the frequency and voltage compensation signals of all DG units, namely $[u^{\omega}_{1,stcn}, u^{V}_{1,stcn}, ..., u^{\omega}_{N,stcn}, u^{V}_{N,stcn}]$.

First, for the input tensor $X(t)$, the spatial convolution module aggregates local spatial information among DGs according to the communication topology. In the implemented STCN, two spatial convolution layers are used. Each spatial convolution is performed along the node dimension with a kernel size of $K_s=3$, and the graph adjacency relationship is used as a binary mask to ensure that each DG only aggregates information from itself and its neighboring DGs. The numbers of output channels of the first and second spatial convolution layers are 32 and 64, respectively. Zero padding is adopted to preserve the node dimension. The rectified linear unit (ReLU) activation function is used after each spatial convolution layer, followed by layer normalization to improve training stability. For the l -th spatial convolution layer, the output can be expressed as:

$$\mathbf{H}_s^{(l)} = \sigma(\mathbf{W}_s^{(l)} *_s \mathbf{H}_s^{(l-1)} + \mathbf{b}_s^{(l)}) \tag{16}$$

where $*_s$ denotes the masked convolution or neighborhood aggregation operation along the spatial node dimension, $W_s^{(l)}$ and $b_s^{(l)}$ are the kernel parameters and bias term of the l -th spatial convolution layer, and

$\sigma(\cdot)$ is the ReLU activation function. In this work, $H_s^{(0)} = X(t)$, and $l = 1, 2$. The spatial convolution kernel size is set to 3, and the hidden channel numbers are set to 32 and 64, respectively. The adjacency mask derived from A is applied during spatial aggregation so that non-neighboring node information is not used. Therefore, the spatial convolution module remains consistent with the distributed communication topology.

After obtaining the spatial feature representation, the temporal convolution module further extracts dynamic features along the time dimension. In the implemented network, three one-dimensional temporal convolution layers are adopted along the time axis. The kernel size of each temporal convolution layer is $K_t = 3$. To enlarge the temporal receptive field while maintaining a compact network size, dilated causal convolutions are used, and the dilation rates of the three temporal convolution layers are set to 1, 2, and 4, respectively. The corresponding output channel numbers are 64, 64, and 32. ReLU activation and layer normalization are applied after each temporal convolution layer. With the time-window length $T = 12$, the above dilation configuration is sufficient to cover the dominant transient dynamics considered in the simulation scenarios. Compared with recurrent neural networks, temporal convolutional structures offer advantages such as stronger parallel computation capability, more stable gradient propagation, and easier modeling of long-range temporal dependencies. The output of the k -th temporal convolution layer can be written as:

$$H_t^{(k)} = \sigma(W_t^{(k)} *_t H_t^{(k-1)} + b_t^{(k)}) \tag{17}$$

where $*_t$ denotes the causal convolution operation along the time dimension, and $W_t^{(k)}$ and $b_t^{(k)}$ are the parameters of the temporal convolution layer. In the above, $H_t^{(0)}$ is the output of the spatial convolution module, and $k = 1, 2, 3$. The temporal convolution layers use causal padding to prevent the controller from using future information. Therefore, the compensation signals at time t are generated only from the current and historical measurements within the sliding time window.

After spatiotemporal feature extraction, global average pooling is applied along the temporal dimension to obtain a compact spatiotemporal feature representation for each DG node. The resulting feature vector is then sent to two fully connected layers for feature fusion and output mapping. The dimensions of the two fully connected layers are 32 and 2, respectively, where the final two outputs correspond to $u_{i,stcn}^{\omega}(t)$ and $u_{i,stcn}^{V}(t)$. Let $z_i(t)$ denote the fused feature vector. Then, the control outputs for the i -th DG are given by:

$$[u_i^{\omega}(t), u_i^{V}(t)] = \phi(\mathbf{z}_i(t)) \tag{18}$$

where $\phi(\cdot)$ denotes the output mapping implemented by fully connected layers. A hyperbolic tangent activation function is used in the final layer, and the output is scaled by the preset compensation limits to satisfy the amplitude constraints. Therefore, the STCN compensation signals are constrained as:

$$u_i^{\omega}(t) \in [u_{\min}, u_{\max}], u_i^{V}(t) \in [u_{\min}, u_{\max}] \tag{19}$$

By constraining the compensation signals within bounded ranges, excessively abrupt control actions can be avoided, thereby improving the stability and safety of the closed-loop control system. Under the above configuration, the STCN used in the simulations contains approximately 3.8×10^4 trainable parameters. This relatively compact size enables real-time forward inference in the secondary control layer. The detailed hyperparameters of the implemented STCN are summarized in Table 1.

Table 1. Detailed hyperparameters of the implemented STCN

Module	Layer	Kernel size	Dilation rate	Output channels / dimension	Activation
Input	Spatiotemporal tensor	—	—	(N×F×T)	—
Spatial convolution	Spatial Conv 1	3	—	32	ReLU
Spatial convolution	Spatial Conv 2	3	—	64	ReLU
Temporal convolution	Temporal Conv 1	3	1	64	ReLU
Temporal convolution	Temporal Conv 2	3	2	64	ReLU
Temporal convolution	Temporal Conv 3	3	4	32	ReLU
Feature fusion	Global average pooling	—	—	32	—
Output mapping	Fully connected layer	—	—	32	ReLU
Output mapping	Fully connected layer	—	—	2 per DG	Tanh

Layer normalization is applied after each convolutional layer. The final tanh output is multiplied by the compensation limits to generate bounded secondary compensation signals.

Distributed Secondary Control Law

In conventional distributed secondary control frameworks, the control input is usually constructed from frequency consensus errors, voltage consensus errors, and reference deviations. Although such approaches have clear physical interpretations and good explainability, their performance is often limited by fixed controller parameters and predefined control structures under complex operating conditions. To address this issue, the STCN is embedded into the distributed secondary control loop as a dynamic compensator, so that the

controller can better adapt to complicated dynamic scenarios while retaining the basic distributed control structure.

Specifically, let $u_{i,conv}^{\omega}$ and $u_{i,conv}^{V}$ denote the conventional distributed secondary control inputs for the i -th DG. Then, the proposed secondary control law is designed as:

$$u_i^{\omega} = u_{i,conv}^{\omega} + u_{i,stcn}^{\omega} \tag{20}$$

$$u_i^{V} = u_{i,conv}^{V} + u_{i,stcn}^{V} \tag{21}$$

where $u_{i,stcn}^{\omega}$ and $u_{i,stcn}^{V}$ are the frequency and voltage cooperative compensation terms generated by the STCN, respectively. Accordingly, the reference update equations under the proposed secondary control can be written as:

$$\omega_i = \omega^* - m_{p_i}(P_i - P_i^*) + u_{i,conv}^{\omega} + u_{i,stcn}^{\omega} \tag{22}$$

$$V_i = V^* - n_{q_i}(Q_i - Q_i^*) + u_{i,conv}^{V} + u_{i,stcn}^{V} \tag{23}$$

This “conventional controller + spatiotemporal compensator” design offers two major advantages. First, the conventional control component provides the basic restoration capability and preserves the physical interpretability of the control law, ensuring that the overall design remains consistent with the standard distributed secondary control framework. Second, the STCN compensation term can adaptively adjust the control action online according to the historical multi-node states, thereby enhancing the controller’s capability to cope with load variations, model uncertainty, and complex coupled dynamics.

To emphasize the cooperative nature of frequency and voltage restoration, this paper does not design two completely independent control networks. Instead, a shared spatiotemporal feature extraction backbone with two output heads is adopted. In other words, the frequency compensation and voltage compensation share the same spatiotemporal representation in the lower layers and are mapped separately to u_i^{ω} and u_i^{V} in the output stage. This design enables the network to explicitly capture the potential coupling between frequency and voltage during joint modeling, thereby improving coordinated restoration performance.

Training and Online Implementation

Considering the real-time and safety requirements of microgrid control, an “offline training + online deployment” strategy is adopted in this paper. To improve the reproducibility of the proposed method, the training dataset construction, optimization settings, validation procedure, and loss-function coefficients are specified in detail in this subsection.

Specifically, a simulation environment covering multiple operating scenarios is first established, including sudden load changes, parameter perturbations, communication delays, and consecutive multi-disturbance events. In this study, 2400 time-domain simulation runs are generated for offline training and evaluation. The scenarios include 800 load-increase cases, 600 load-decrease cases, 400 DG-parameter perturbation cases, 400 communication-delay cases, and 200 combined-disturbance cases. In each simulation run, the load variation level is randomly selected from 10% to 30%, the DG parameter perturbation is randomly selected from -15% to $+15\%$, and the communication delay is randomly selected from 20 ms to 100 ms. The disturbance occurrence time is randomly sampled between 0.8 s and 1.5 s to avoid overfitting to a fixed disturbance instant. The sampling period is 10 ms and the simulation horizon is 8 s. Therefore, each simulation run produces 800 sampling instants. By applying a sliding time window with $T = 12$, approximately 1.89×10^6 spatiotemporal samples are obtained before data splitting.

It should be noted that the STCN is not assumed to learn universal physical laws of the microgrid. Its generalization capability mainly depends on the coverage of the offline training scenarios. To reduce overfitting to a single transient pattern, the training data are generated with randomized disturbance magnitudes, disturbance occurrence times, parameter perturbations, and communication delays, and the dataset is divided at the simulation-trajectory level rather than at the individual-sample level. Therefore, the validation and test trajectories are not identical to the training trajectories.

The generated samples are divided into training, validation, and test datasets according to a ratio of 70%, 15%, and 15%, respectively. The division is performed at the simulation-run level rather than at the individual-sample level, so that samples from the same disturbance trajectory do not appear simultaneously in the training and validation/test sets. This strategy helps provide a more reliable evaluation of the generalization capability of the trained STCN under unseen disturbance trajectories. All input features are normalized using the mean and standard deviation calculated from the training dataset, and the same normalization parameters are used during validation, testing, and online inference.

To ensure that the network outputs are aligned with the control objectives, the loss function is designed as a comprehensive performance index that simultaneously considers frequency restoration error, voltage restoration error, dynamic performance, and control smoothness, i.e.,

$$\mathcal{L} = \alpha\mathcal{L}_{\omega} + \beta\mathcal{L}_{V} + \gamma\mathcal{L}_{d} + \eta\mathcal{L}_{u} \tag{24}$$

where L_{ω} and L_{V} denote the loss terms associated with frequency deviation and voltage deviation, respectively; L_{d} denotes the dynamic performance term, which reflects restoration speed, overshoot, oscillation level, and inter-node consistency error; L_{u} denotes the penalty term associated with the rate of change and magnitude of the control input. These two terms are included to reduce the risk of poorly timed or excessively oscillatory compensation signals, so that the STCN output is not optimized only for instantaneous error reduction but also for smooth transient behavior. $\alpha, \beta, \gamma, \eta$ are the corresponding weighting coefficients. In the simulations, the weighting coefficients are set as $\alpha = 1.0$, $\beta = 1.0$, $\gamma = 0.2$, and $\eta = 0.01$. The relatively larger weights of L_{ω} and L_{V} emphasize the primary restoration objectives, while L_{d} is assigned a moderate weight to suppress oscillations and improve dynamic consistency. The control-smoothness penalty L_{u} is assigned a smaller weight to avoid excessive control variation without weakening the main restoration capability.

The training targets are generated from the desired compensation signals obtained by minimizing the restoration-oriented performance index over the offline simulation trajectories. In this way, the STCN is trained in a supervised manner to approximate the compensation policy that reduces frequency and voltage deviations while maintaining smooth control actions. The STCN is trained using the Adam optimizer. The initial learning rate is set to 1×10^{-3} , and a learning-rate decay factor of 0.5 is applied if the validation loss does not decrease for 10 consecutive epochs. The batch size is set to 128, and the maximum number of training epochs is 200. Early stopping is adopted when the validation loss does not improve for 20 consecutive epochs. The model with the lowest validation loss is selected for online deployment.

After training is completed, the resulting STCN parameters are fixed and deployed in the local controller of each DG. During online operation, each DG constructs its input window $X_i(t)$ in real time according to local sampled measurements and received neighborhood information. The current compensation signals $u_{i,stcn}^{\omega}$ and $u_{i,stcn}^{V}$ are then obtained through forward inference of the STCN and superimposed onto the conventional secondary control terms to form the final control inputs. Since the online stage only involves forward

propagation, the computational burden is much lower than that of online training or optimization. In the implemented STCN, the number of trainable parameters is approximately 3.8×10^4 , and each inference step only requires a fixed sequence of convolutional and fully connected operations. In the present implementation, the average inference time of one STCN forward pass was measured to be below 1 ms on a desktop CPU equipped with an Intel i7 processor and 16 GB RAM, which is lower than the 10 ms control sampling period. Therefore, the proposed controller can meet the sampling interval in the tested implementation. Nevertheless, inference latency and timing jitter should be further considered when the method is deployed on low-cost embedded controllers.

In summary, the proposed STCN-based distributed secondary cooperative restoration control method does not directly replace the original control structure with a standalone black-box neural controller. Instead, it embeds the neural network into the secondary control loop as an intelligent compensation module tailored for multi-node spatiotemporal dynamics. This design not only enhances the controller's ability to characterize complex dynamic behavior, but also provides a clear structural basis for the subsequent closed-loop stability analysis and performance validation.

STABILITY AND CONVERGENCE ANALYSIS

Closed-Loop System Representation

Based on the system model in Section 2 and the control law proposed in Section 3, the closed-loop dynamics of the microgrid under secondary control can be represented as a coupled system consisting of the physical plant, the conventional distributed secondary controller, and the STCN-based dynamic compensator. For convenience of analysis, define the state vector of the i -th DG as:

$$\mathbf{s}_i(t) = [\Delta\omega_i(t), \Delta V_i(t)]^\top \tag{25}$$

and stack the states of all DG units into a global state vector:

$$\mathbf{s}(t) = [\mathbf{s}_1^\top(t), \mathbf{s}_2^\top(t), ..., \mathbf{s}_N^\top(t)]^\top \tag{26}$$

where $\Delta\omega_i(t) = \omega_i(t) - \omega^*$ and $\Delta V_i(t) = V_i(t) - V^*$. According to the proposed "conventional controller + STCN compensator" structure, the secondary control input of the i -th DG can be written as:

$$\mathbf{u}_i(t) = \mathbf{u}_{i,conv}(t) + \mathbf{u}_{i,stcn}(t) \tag{27}$$

Where:

$$\mathbf{u}_i(t) = [u_i^{\omega}(t), u_i^{V}(t)]^{\top} \tag{28}$$

$$\mathbf{u}_{i,conv}(t) = [u_{i,conv}^{\omega}(t), u_{i,conv}^{V}(t)]^{\top} \tag{29}$$

$$\mathbf{u}_{i,stcn}(t) = [u_{i,stcn}^{\omega}(t), u_{i,stcn}^{V}(t)]^{\top} \tag{30}$$

Then, the overall closed-loop system can be abstractly expressed as:

$$\dot{\mathbf{s}}(t) = \mathbf{F}(\mathbf{s}(t)) + \mathbf{G}(\mathbf{s}(t))\mathbf{u}_{conv}(t) + \mathbf{G}(\mathbf{s}(t))\mathbf{u}_{stcn}(t) + \mathbf{d}(t) \tag{31}$$

where $F(\cdot)$ denotes the nonlinear state evolution of the microgrid under plant dynamics and primary droop control, $G(\cdot)$ is the control input matrix, $d(t)$ represents external disturbances such as load variations, parameter perturbations, and communication errors, and $u_{conv}(t)$ and $u_{stcn}(t)$ denote the conventional distributed secondary control input and the STCN compensation input, respectively.

This representation shows that the proposed method does not alter the basic control structure of the original microgrid, but rather introduces a spatiotemporal feature-driven dynamic compensation channel into the conventional secondary control loop. Therefore, the stability analysis of the closed-loop system can be reduced to investigating how the STCN compensation term affects the boundedness and convergence properties of the overall system, given that the conventional control term already provides basic restoration capability.

To avoid ambiguity in the stability discussion, the following assumptions are made for the subsequent analysis. The communication graph is assumed to be undirected and connected. In the considered operating region, the microgrid dynamics $F(s)$ and the input matrix $G(s)$ are locally Lipschitz, and $G(s)$ is bounded. The conventional distributed secondary controller is assumed to be properly designed such that the nominal closed-loop system without the STCN compensator is input-to-state stable with respect to the external disturbance $d(t)$. That is, there exists a continuously differentiable Lyapunov function $V(s)$ satisfying:

$$c_1 \parallel s \parallel^2 \leq V(s) \leq c_2 \parallel s \parallel^2 \tag{32}$$

and

$$\dot{V}(s) \leq -c_3 \parallel s \parallel^2 + c_4 \parallel d(t) \parallel^2 \tag{33}$$

where c_1, c_2, c_3, c_4 are positive constants. In addition, the external disturbance and the STCN output are bounded, namely $\parallel d(t) \parallel \leq \bar{d}$ and $\parallel u_{stcn}(t) \parallel \leq \bar{u}$. These assumptions explicitly define the scope of the stability analysis. The proposed STCN is therefore analyzed as a bounded performance-enhancing compensator built upon a stabilizing distributed secondary controller, rather than as an independent stabilizing controller.

Boundedness of the STCN Compensation Signals

To guarantee safe operation of the closed-loop control system, it is first necessary to show that the compensation signals generated by the STCN remain bounded under bounded inputs. According to the network design in Section 3, the input of the STCN is composed of local measurements and neighborhood information over a finite time window, i.e.,

$$\mathbf{X}_i(t) = [\tilde{\mathbf{x}}_i(t-T+1), \tilde{\mathbf{x}}_i(t-T+2), ..., \tilde{\mathbf{x}}_i(t)] \tag{34}$$

Since the frequency deviation, voltage deviation, and power measurements in practical microgrids remain bounded within normal operating ranges, and the neighborhood information transmitted over the communication network is also physically constrained, it is reasonable to assume that there exists a positive constant $M_x > 0$ such that:

$$\parallel \mathbf{X}_i(t) \parallel \leq M_x \tag{35}$$

for any $t \geq 0$.

On the other hand, the proposed STCN consists of a finite number of convolutional layers, nonlinear activation functions, and fully connected mappings, and all network weights are fixed finite values after training. Moreover, explicit saturation or amplitude constraints are imposed at the output layer. Therefore, for any bounded input $X_i(t)$, there exist positive constants $M_u^{\omega} > 0$ and $M_u^V > 0$ such that:

$$| u_{i,stcn}^{\omega}(t) | \leq M_u^{\omega} \tag{36}$$

$$| u_{i,stcn}^{V}(t) | \leq M_u^{V} \tag{37}$$

for all $i = 1, 2, ..., N$ and $t \geq 0$.

Hence, the STCN compensator constitutes a bounded-input bounded-output (BIBO) mapping. This property guarantees that, under bounded states and measurement signals, the neural network will not generate unbounded control inputs, thereby preventing excessively large compensation terms from destabilizing the original secondary control loop.

Since the STCN consists of a finite number of convolutional and fully connected layers with continuous activation functions, its input-output mapping is locally Lipschitz over the compact operating region considered in this study. Together with the output saturation layer, this property allows the STCN compensator to be treated as a bounded auxiliary input in the subsequent ISS-based analysis.

Closed-Loop Stability Analysis

Under the action of the conventional distributed secondary controller alone, if the communication graph is connected and the controller parameters satisfy the corresponding design conditions, the frequency and voltage errors can be driven to zero or confined within a sufficiently small neighborhood. In this paper, the STCN compensation term is introduced on top of this baseline controller, and its essential role is to provide a bounded dynamic correction to the conventional control input. Therefore, the stability of the closed-loop system can be analyzed by treating the STCN compensation term as an additional bounded input and invoking the concept of input-to-state stability (ISS).

Based on the above assumptions, the influence of the STCN compensator can be explicitly included in the Lyapunov analysis. Since $G(s)$ is bounded in the considered operating region and the STCN output is constrained by the saturation layer, there exists a positive constant c_5 such that the additional term caused by $u_{stcn}(t)$ satisfies

$$\dot{V}(s) \leq -c_3 \parallel s \overset{2}{\parallel} + c_4 \parallel d(t) \overset{2}{\parallel} + c_5 \parallel u_{stcn}(t) \overset{2}{\parallel} . \tag{38}$$

Using $\parallel d(t) \parallel \leq \bar{d}$ and $\parallel u_{stcn}(t) \parallel \leq \bar{u}$, one obtains

$$\dot{V}(s) \leq -c_3 \parallel s \parallel^2 + c_4 \bar{d}^2 + c_5 \bar{u}^2 \tag{39}$$

Therefore, $\dot{V}(s) < 0$ when

$$\parallel s \parallel > \sqrt{\frac{c_4 \bar{d}^2 + c_5 \bar{u}^2}{c_3}}. \tag{40}$$

This indicates that the closed-loop state under the proposed STCN-assisted secondary controller is uniformly ultimately bounded. The frequency and voltage deviations converge to a residual neighborhood whose size is related to the disturbance bound, the STCN output bound, and the dissipation margin of the baseline distributed controller. Therefore, the boundedness of the STCN output alone is not used as an independent stability guarantee; rather, it is combined with the ISS property of the baseline controller to establish practical closed-loop stability.

It should be emphasized that the above ISS-based result only establishes practical closed-loop stability and boundedness. It does not, by itself, prove that the STCN compensation necessarily improves transient performance. A bounded auxiliary compensation signal may still lead to undesirable oscillations if it is not properly trained or timed. Therefore, the performance improvement of the proposed method is not inferred solely from the boundedness of $u_{stcn}(t)$, but is supported by the restoration-oriented training objective and the comparative simulation results presented in Section 5.

Convergence and Cooperative Restoration Performance

Based on the above analysis, the STCN-assisted controller preserves practical closed-loop stability under the stated assumptions. It should be noted that this theoretical result concerns boundedness and convergence to a residual neighborhood, while the improvement in transient response is evaluated through the restoration-oriented training objective and the comparative simulations. Therefore, the boundedness of the STCN output is a stability-preserving condition, not an independent proof of performance improvement.

From the perspective of the convergence mechanism, conventional secondary control mainly relies on current errors and neighborhood consensus information to drive the restoration process. By contrast, the proposed STCN compensation term further exploits the state trajectories over a historical time window to extract the variation trend under disturbances and the correlation pattern among multiple nodes. When a sudden load

change or node-state deviation occurs, the STCN can identify the error growth trend from the spatiotemporal features and generate more targeted corrective actions, thereby accelerating the convergence of frequency and voltage errors toward the equilibrium point while reducing overshoot and oscillation during the transient process.

In addition, since frequency restoration and voltage restoration share the same spatiotemporal representation in the lower layers, the proposed controller can simultaneously account for the potential coupling between the active-power/frequency regulation channel and the reactive-power/voltage regulation channel within a unified framework. This means that when changes in one class of states indirectly affect the other control objective, the network can automatically adjust the relative strengths of the two compensation channels through joint feature mapping, thereby enhancing the cooperative restoration capability of frequency and voltage.

Based on the above analysis, the following conclusion can be drawn: under a connected communication topology, a baseline conventional distributed secondary controller with basic stability guarantees, bounded external disturbances, and bounded STCN outputs. Under the explicitly stated assumptions, the proposed STCN-assisted control framework ensures uniform ultimate boundedness of the closed-loop frequency and voltage deviation states. The residual convergence neighborhood depends on the external disturbance bound, the STCN output bound, and the dissipation margin of the baseline distributed secondary controller. Therefore, the proposed method should be interpreted as a stability-preserving performance enhancement framework built upon a stabilizing distributed controller, rather than as an unconditional neural-network-based stabilizing controller.

CASE STUDIES AND PERFORMANCE EVALUATION

Simulation Setup and Test Scenarios

To validate the effectiveness of the proposed STCN-based distributed secondary cooperative restoration control method, case studies are carried out on an islanded AC microgrid simulation platform established in MATLAB/Simulink. The microgrid is modeled using averaged voltage-source inverter models with output LC filters and droop-controlled primary regulation. Since this paper focuses on secondary frequency and voltage restoration rather than high-frequency switching behavior, the switching dynamics of power electronic devices are not explicitly modeled. The simulation is performed using a fixed-step discrete solver with an electrical simulation step size of 1×10^{-4} s, while the secondary controller and the STCN inference module

are updated every 10 ms. Therefore, the sampling period in Table 2 refers to the control sampling period rather than the numerical solver step size.

Table 2. Main simulation settings and system parameters

Parameter	Value
Simulation platform	MATLAB/Simulink
Model type	Averaged VSI with (LC) filter
Solver and step size	Fixed-step discrete, (1×10^{-4}) s
Control sampling period	10 ms
Rated frequency / voltage	50 Hz / 1.0 p.u.
DG units	4
Electrical line set	εe={(1,2),(2,3),(3,4)})
Communication link set	εc={(1,2),(2,3),(3,4)})
Line impedances	(Z12=0.010+j0.050) p.u.; (Z23=0.012+j0.055) p.u.; (Z34=0.010+j0.050) p.u.
Filter parameters	(Lf=1.8) mH, (Cf=25μF)
Droop coefficients	(mp=0.002), (nq=0.010) p.u./p.u.
Time-window length	12 steps
Disturbance time / horizon	1.0 s / 8 s

The test system consists of four inverter-based DG units, local loads, distribution lines, and a communication network. The electrical topology is represented by the line set $\mathcal{E}_e = \{(1,2),(2,3),(3,4)\}$, and the communication topology is selected as $\mathcal{E}_c = \{(1,2),(2,3),(3,4)\}$. The corresponding line impedances and main simulation parameters are summarized in Table 2. Standard droop control is employed in the primary layer, while the secondary layer is configured with three different methods for comparison, namely, the conventional distributed secondary control, an improved distributed control method, and the proposed STCN-based method.

In addition to the microgrid simulation settings, the main implementation parameters of the STCN are also specified for reproducibility. The sampling period is 10 ms, and the sliding time-window length is 12 sampling steps. The STCN contains two spatial convolution layers, three temporal convolution layers, and two fully connected layers. The temporal dilation rates are set to 1, 2, and 4, respectively. ReLU is used as the activation function in hidden layers, while tanh is used in the output layer to impose bounded compensation signals. The total number of trainable parameters is approximately 3.8×10^4 . During online operation, only forward inference is performed, and the network parameters remain fixed after offline training.

As shown in table 3. The dataset split is performed at the simulation-run level to avoid trajectory-level data leakage. The model with the lowest validation loss is used in all test cases reported in this paper.

Table 3. Training settings of the STCN

Parameter	Value
Number of simulation runs	2400
Load-increase cases	800
Load-decrease cases	600
DG-parameter perturbation cases	400
Communication-delay cases	400
Combined-disturbance cases	200
Load variation range	10%–30%
DG parameter perturbation range	(−15%) to (+15%)
Communication delay range	20–100 ms
Disturbance time	Randomly selected from 0.8–1.5 s
Dataset split	70% training, 15% validation, 15% testing
Optimizer	Adam
Initial learning rate	(1×10^{-3})
Batch size	128
Maximum epochs	200
Early stopping patience	20 epochs
Learning-rate decay	0.5 after 10 stagnant validation epochs
Loss weights	(α=1.0,β=1.0,γ=0.2,η=0.01)

To evaluate the proposed method from both dynamic restoration and robustness perspectives, four representative operating scenarios are considered, involving load disturbances, parameter perturbations, and communication constraints. The detailed test cases are listed in Table 4.

Table 4. Test cases for performance evaluation

Case	Scenario	Purpose
Case 1	20% step load increase	Dynamic restoration test
Case 2	20% step load decrease	Recovery symmetry test
Case 3	DG parameter perturbation (+15%)	Robustness to model uncertainty
Case 4	Communication delay (80 ms) + load disturbance	Communication robustness test

In terms of evaluation criteria, this paper mainly focuses on the maximum frequency deviation, frequency recovery time, maximum voltage deviation, voltage recovery time, overshoot, and power-sharing error. Here,

the recovery time is defined as the time required for the system state to enter and remain within a prescribed tolerance band around the nominal value. These metrics provide a comprehensive basis for assessing the controller performance in transient response speed, steady-state accuracy, and overall robustness.

Frequency and Voltage Restoration under Load Increase

Case 1 is first considered, where a 20% step load increase is applied at $t = 1.0$ s to examine the restoration performance of different methods under a typical transient disturbance. Figure 1 presents the dynamic response of frequency deviation under the three control strategies, while Figure 2 shows the corresponding voltage deviation restoration curves.

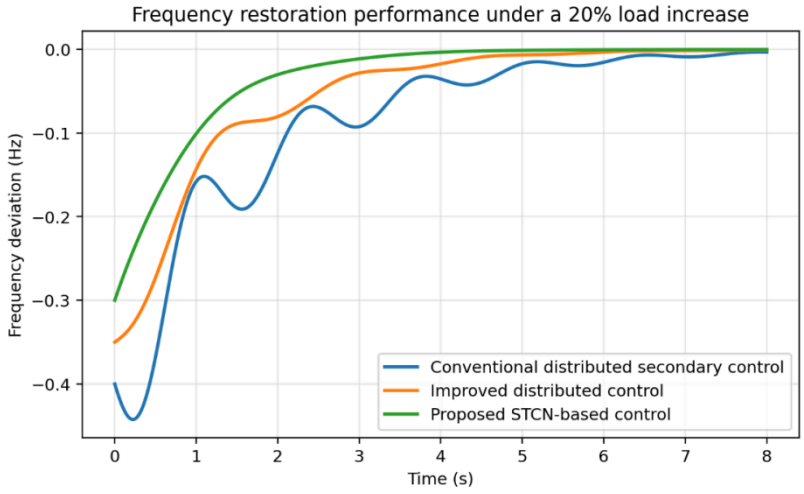

Figure 1. Frequency restoration performance under a 20% load increase

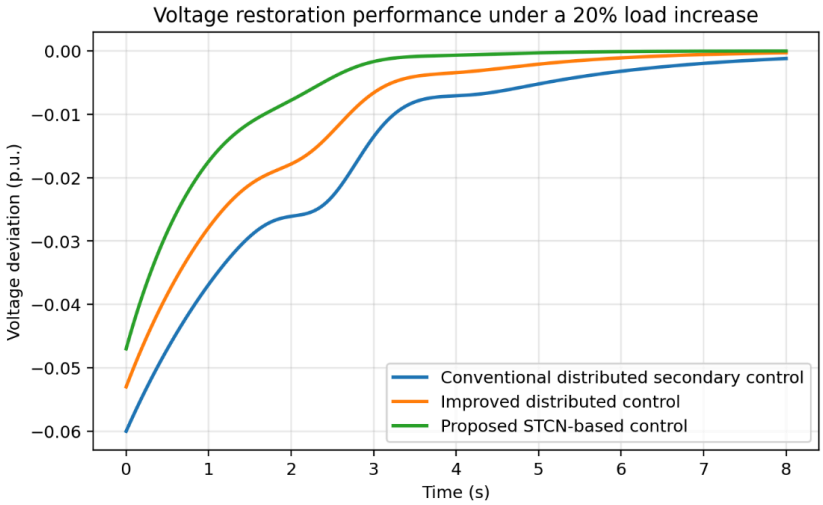

Figure 2. Voltage restoration performance under a 20% load increase

As observed from Fig. 1, all three methods are able to drive the system frequency back toward its nominal value after the disturbance, but the restoration processes differ significantly. The conventional distributed secondary control exhibits a relatively large frequency drop after the disturbance, accompanied by more pronounced oscillations and a slower convergence process. The improved distributed control outperforms the conventional one in terms of restoration speed and oscillation suppression, yet noticeable transient fluctuations still remain. By contrast, the proposed STCN-based method shows a faster frequency restoration rate and smaller transient oscillations, indicating that the controller can more effectively exploit the spatiotemporal dynamics during disturbance evolution and generate more targeted compensation for frequency deviations.

A similar trend can be observed in the voltage restoration results shown in Fig. 2. The conventional method leads to a larger voltage dip and a longer recovery period following the load increase. Although the improved distributed method enhances the transient voltage response to some extent, its performance is still constrained by its fixed control structure. In comparison, the proposed STCN-based method demonstrates better characteristics in terms of voltage deviation magnitude, recovery speed, and transient smoothness. This suggests that the shared spatiotemporal feature extraction mechanism can simultaneously enhance the regulation capability of both the frequency channel and the voltage channel, thereby improving the overall performance of secondary cooperative restoration control.

Quantitative Performance Comparison

To provide a more direct comparison of the control performance, Table 5 summarizes the major performance indices of the three methods under Case 1.

Table 5. Performance comparison under Case 1

Method	Max frequency deviation (Hz)	Frequency recovery time (s)	Max voltage deviation (p.u.)	Voltage recovery time (s)	Overshoot (%)	Power-sharing error (%)
Conventional distributed secondary control	0.42	4.8	0.060	5.2	8.6	4.8
Improved distributed control	0.36	3.5	0.053	3.9	5.1	3.2
Proposed STCN-based control	0.30	2.1	0.047	2.4	2.3	1.7

As shown in Table 5, the proposed STCN-based method outperforms the two benchmark methods in all key performance indices. Compared with the conventional distributed secondary control, the proposed method

reduces the maximum frequency deviation from 0.42 Hz to 0.30 Hz and shortens the frequency recovery time from 4.8 s to 2.1 s. Meanwhile, the maximum voltage deviation is reduced from 0.060 p.u. to 0.047 p.u., and the voltage recovery time is shortened from 5.2 s to 2.4 s. In addition, the STCN-based method also achieves better performance in terms of overshoot and power-sharing error, indicating that it not only improves the restoration speed of frequency and voltage, but also maintains better coordinated control quality with less impact on power-sharing characteristics.

These results demonstrate that, by jointly modeling the spatial coupling among multiple nodes and the temporal evolution of system dynamics, the proposed controller is able to go beyond the conventional paradigm based solely on instantaneous error correction, thereby achieving more significant advantages in both restoration accuracy and transient performance.

Robustness under Communication Delay and Parameter Perturbation

To further verify the robustness of the proposed method under more challenging operating conditions, Case 4 is considered, where an 80 ms communication delay is introduced together with load disturbance and parameter perturbation. Figure 3 shows the frequency restoration curves of different methods under this scenario.

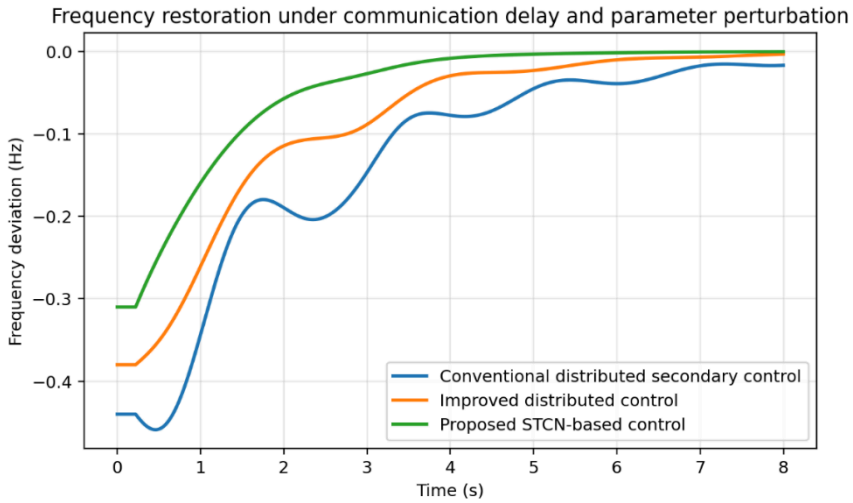

Figure 3. Frequency restoration under communication delay and parameter perturbation

As can be seen from Fig. 3, under the combined effects of communication delay and parameter uncertainty, the dynamic performance of the conventional distributed secondary control degrades significantly, as reflected by a larger frequency deviation, longer recovery time, and stronger oscillatory behavior. This indicates

that a fixed-parameter controller has limited adaptability to rapidly changing system dynamics under complex conditions. Although the improved distributed method alleviates these issues to some extent, its restoration process is still noticeably affected by the communication constraints. In contrast, the proposed STCN-based method maintains a relatively fast convergence speed and a smaller oscillation amplitude, demonstrating stronger robustness against complex disturbances and communication uncertainty.

The reason lies in the fact that the STCN controller does not rely solely on instantaneous local deviation information when generating the online compensation signals. Instead, it comprehensively utilizes the historical state trajectories within the time window as well as the coupling relationships among multiple nodes. Therefore, when communication delay or model perturbation leads to accumulated control errors, the network can adjust the compensation signals in a timely manner through spatiotemporal feature mapping, thereby enhancing the system's adaptability to uncertainty.

Discussion of Results

Based on the above case studies, several conclusions can be drawn. First, under typical load disturbance conditions, the proposed STCN-based distributed secondary control method exhibits faster dynamic response and smaller transient deviations in both the frequency and voltage channels, demonstrating strong cooperative restoration capability. Second, according to the quantitative performance comparison, the proposed method consistently outperforms the benchmark methods in terms of recovery time, overshoot, and power-sharing error, indicating that it not only improves restoration speed but also enhances the smoothness and coordination of the control process. Finally, under complex conditions involving communication delay and parameter perturbation, the proposed method still maintains stable and superior dynamic performance, which verifies the robustness of the proposed control framework under uncertainty.

Overall, the simulation results are consistent with the theoretical analysis presented in the previous sections. Since the proposed method explicitly exploits the spatial correlation among multiple DG nodes and the temporal evolution characteristics of disturbance responses through the STCN, the resulting secondary compensation signals can better match the dynamic requirements of the microgrid. This is the key reason why the proposed method achieves improved control performance in the cooperative restoration problem of frequency and voltage.

DISCUSSION

Although the case studies presented in the previous section demonstrate that the proposed STCN-based distributed secondary cooperative restoration control method achieves superior performance in frequency and voltage restoration, it is still necessary to further discuss its applicability, the underlying sources of its advantages, and its possible limitations from both methodological and engineering perspectives.

First, from the viewpoint of control mechanism, the key strength of the proposed method does not simply lie in the introduction of a neural network, but rather in its ability to jointly model the spatial coupling characteristics and temporal dynamic features inherent in the secondary control problem of microgrids. In an islanded microgrid composed of multiple DG units, the nodes interact through both electrical interconnections and communication topology, which makes the overall system dynamics strongly networked in nature. At the same time, frequency and voltage restoration are typical transient evolution processes, whose control performance depends not only on the instantaneous deviations but also on the historical state trajectories following a disturbance. Conventional distributed secondary control methods mainly construct fixed control laws based on local errors or neighborhood consensus information, whereas the proposed method employs a shared spatiotemporal feature extraction mechanism that allows the controller to perceive the system operating condition in a higher-dimensional manner. This provides richer information support for the coordinated regulation of frequency and voltage.

Second, from an engineering implementation perspective, the proposed structure adopts a “conventional controller + STCN compensator” architecture instead of directly replacing the existing control framework with a purely data-driven controller. This design choice is practically meaningful. On the one hand, the conventional distributed secondary controller preserves the basic physical structure and interpretability of the control law, allowing the overall method to remain compatible with the hierarchical control architecture of existing microgrids. On the other hand, the STCN compensator acts as an auxiliary regulation module whose main role is to enhance dynamic performance and robustness under complex operating conditions. This helps alleviate engineering concerns regarding the stability and safety of purely black-box control strategies. Therefore, from the deployment point of view, the proposed approach is better regarded as a “data-enhanced control framework” rather than a complete replacement of conventional control theory.

Furthermore, the proposed method has promising application potential for systems with high penetration of inverter-based distributed generation. As the degree of power-electronic interfacing continues to increase

in future power systems, the operational dynamics of microgrids become increasingly coupled, fast-varying, and uncertain. Under such conditions, conventional controllers based on fixed parameters or linearized approximations may suffer from performance degradation. By contrast, controllers equipped with spatiotemporal feature extraction capability are, in principle, better suited for handling multi-node, multivariable, and strongly coupled dynamic control problems. Therefore, the control framework proposed in this paper is not only relevant to secondary restoration control in islanded microgrids, but also provides a methodological basis for future extensions to more complex scenarios, such as grid-connected/islanded mode transitions, auxiliary energy management control, and coordinated control of multiple microgrids.

Nevertheless, this study still has several limitations. First, the performance of the STCN depends on the coverage and quality of the training data. If the training dataset does not adequately represent practical operating conditions, the generalization capability of the network under unseen scenarios may be limited. In particular, the present STCN is trained and tested under a fixed four-DG topology with randomized disturbances and parameter variations. For substantially changed network topologies, newly added DG units, or strong unmodeled nonlinearities beyond the training range, the controller may require retraining, fine-tuning, or an additional topology-adaptive mechanism. Therefore, the proposed method should be interpreted as a data-enhanced secondary control approach with scenario-dependent generalization, rather than a topology-invariant controller that automatically applies to arbitrary microgrid configurations. Second, although only forward inference is required during online operation, the proposed method remains more complex than conventional PI- or consensus-based controllers in terms of computational burden and parameter configuration, which may impose higher requirements on the controller hardware platform and communication quality. In addition, the validation in this work is mainly conducted in a simulation environment, and further verification on hardware-in-the-loop platforms or physical experimental systems has not yet been carried out. Therefore, future research may focus on lightweight network design, online adaptive updating mechanisms, and experimental implementation, so as to further improve the engineering applicability and practical credibility of the proposed method.

It should also be noted that neural-network inference introduces additional computation time and possible timing jitter compared with conventional PI- or consensus-based controllers. Although the implemented STCN is compact and its measured inference time is below the 10 ms control sampling period in this study, the same latency cannot be automatically guaranteed on all embedded hardware platforms. Therefore, practical

deployment should benchmark the inference time on the target controller, and techniques such as model pruning, quantization, hardware acceleration, or latency compensation may be required. Further hardware-in-the-loop and experimental validation will be considered in future work.

CONCLUSION

This paper has proposed a spatiotemporal convolutional network-based distributed secondary cooperative restoration control method to address the insufficient coordinated control performance in frequency and voltage restoration of islanded microgrids. First, within the hierarchical control framework of microgrids, a system model incorporating primary droop control, distributed communication topology, and secondary restoration objectives was established, and the coordinated restoration problem of frequency and voltage was formulated as a distributed control problem based on local measurements and neighborhood information. On this basis, a spatiotemporal feature representation tailored for the dynamic coupling among multiple DG units was constructed, and an STCN control framework consisting of spatial convolution, temporal convolution, and a dual-output compensation structure was designed to generate online secondary compensation signals for frequency and voltage restoration.

From the theoretical perspective, the boundedness of the STCN compensation signals and the stability of the closed-loop system were analyzed based on the closed-loop system representation. The analysis shows that, under explicitly stated assumptions on the baseline distributed secondary controller, bounded disturbances, and constrained STCN outputs, the proposed closed-loop system is uniformly ultimately bounded, and the frequency and voltage deviations converge to a residual neighborhood of the equilibrium point. From the case-study perspective, comparative simulations were conducted under multiple representative scenarios, including load disturbances, parameter perturbations, and communication delays. The results demonstrate that the proposed method consistently outperforms the benchmark methods in terms of maximum frequency deviation, maximum voltage deviation, recovery time, overshoot, and power-sharing error, thereby confirming its effectiveness in improving both the dynamic performance and robustness of cooperative frequency and voltage restoration.

Overall, the findings of this paper indicate that incorporating node-correlation information and finite-window temporal state variations into distributed secondary control can reduce transient deviations, shorten recovery time, and improve disturbance rejection in the tested microgrid scenarios. Compared with conventional methods based on fixed control structures, the proposed approach can make more effective use of the spatial

correlation information in multi-node systems and the temporal dynamic information during disturbance evolution, thereby achieving faster, smoother, and more robust restoration control. Future work will further consider event-triggered communication mechanisms, lightweight network deployment, and hardware experimental validation to enhance the practical applicability of the proposed method in real microgrid scenarios.

Author Contributions

Conceptualization – Zhou ZY; methodology – Zhou ZY; formal analysis – Zhou ZY; investigation – Zhou ZY; resources – Zhou ZY; writing-original draft preparation – Zhou ZY; writing-review and editing – Zhou ZY; visualization – Zhou ZY; supervision – Zhou ZY. All authors have read and agreed to the published version of the manuscript.

Conflicts of Interest

The author declares no conflict of interest.

Funding

This research received no external funding.

Acknowledgements

Not applicable.

REFERENCES

[1] Peng FZ, Liu C, Li Y, Jain AK, Vinnikov D. Envisioning the future renewable and resilient energy grids—A power grid revolution enabled by renewables, energy storage, and energy electronics. IEEE Journal of Emerging and Selected Topics in Industrial Electronics. 2023; 5(1):8-26. doi: 10.1109/JESTIE.2023.3343291

[2] Georgious R, Refaat R, Garcia J, Daoud AA. Review on energy storage systems in microgrids. Electronics. 2021; 10(17):2134. doi: 10.3390/electronics10172134

[3] Asri R, Aki H, Kodaira D. Optimal operation of shared energy storage on islanded microgrid for remote communities. Sustainable Energy, Grids and Networks. 2023; 35:101104. doi: 10.1016/j.segan.2023.101104

[4] Karamov DN, Ilyushin PV, Suslov KV. Electrification of rural remote areas using renewable energy sources: Literature review. Energies. 2022; 15(16):5881. doi: 10.3390/en15165881

[5] Hasheminasab S, Alzayed M, Chaoui H. A review of control techniques for inverter-based distributed energy resources applications. Energies. 2024; 17(12):2940. doi: 10.3390/en17122940

[6] Sahoo AK, Mahmud K, Crittenden M, Ravishankar J, Padmanaban S, Blaabjerg F. Communication-less primary and secondary control in inverter-interfaced AC microgrid: An overview. IEEE Journal of Emerging and Selected Topics in Power Electronics. 2020; 9(5):5164-5182. doi: 10.1109/JESTPE.2020.2974046

[7] Ahmed M, Meegahapola L, Vahidnia A, Datta M. Stability and control aspects of microgrid architectures comprehensive review. IEEE access. 2020; 8:144730-144766. doi: 10.1109/ACCESS.2020.3014977

[8] Ahmed K, Seyedmahmoudian M, Mekhilef S, Mubarak NM, Stojcevski A. A review on primary and secondary controls of inverter-interfaced microgrid. Journal of Modern Power Systems and Clean Energy. 2020; 9(5):969-985. doi: 10.35833/MPCE.2020.000068

[9] Rodriguez-Martinez OF, Andrade F, Vega-Penagos CA, Luna AC. A review of distributed secondary control architectures in islanded-inverter-based microgrids. Energies. 2023; 16(2):878. doi: 10.3390/en16020878

[10] Ge X, Han Q, Ding L, Wang YL, Zhang XM. Dynamic event-triggered distributed coordination control and its applications: A survey of trends and techniques. IEEE Transactions on Systems, Man, and Cybernetics: Systems. 2020; 50(9):3112-3125. doi: 10.1109/TSMC.2020.3010825

[11] Liu Y, Zhang W, Sun Y, Su M, Xu G, Dan H. Review and comparison of control strategies in active power decoupling. IEEE Transactions on Power Electronics. 2021; 36(12):14436-14455. doi: 10.1109/TPEL.2021.3087170

[12] Issa W, Sharkh S, Abusara M. A review of recent control techniques of drooped inverterased AC microgrids. Energy Science & Engineering. 2024; 12(4):1792-1814. doi: 10.1002/ese3.1670

[13] Machado SDJM, Da Silva SAO, De Almeida Monteiro JRB, Sampaio LP, De Oliveira AA. Analysis of a multifunctional inverter active-filtering function influence on the small-signal stability of inverter-based islanded AC microgrids. IEEE Transactions on Industrial Electronics. 2022; 70(8):8108-8117. doi: 10.1109/TIE.2022.3222630

[14] Hussaini H, Yang T, Gao Y, Wang C, Urrutia M, Bozhko S. Optimal droop control design using artificial intelligent techniques for electric power systems of more-electric aircraft. IEEE Transactions on Transportation Electrification. 2023; 10(1):2192-2206. doi: 10.1109/TTE.2023.3271763

[15] Jackson R, Zulkifli SA, Benbouzid M, Salimin S, Khan MH, Elhassan G, Pathan E. A comprehensive motivation of multilayer control levels for microgrids: Synchronization, voltage and frequency restoration perspective. Applied Sciences. 2020; 10(23):8355. doi: 10.3390/app10238355